SUPPORTING INFORMATION

Metal-Support Interactions in Fe-Cu-K Admixed with SAPO-34 Catalysts for Highly Selective Transformation of CO_2 and H_2 into Lower Olefins

Jie Ding[1,2], Qiang Liu[1], Run-ping Ye[4], Weibo Gong[2], Fan Zhang[5], Xiang He[6], Yulong Zhang[8], Qin Zhong[1*], Morris D. Argyle[3*], Maohong Fan[2,7*]

[1]*School of Chemical Engineering, Nanjing University of Science and Technology, Nanjing, Jiangsu 210094, P. R. China, tonlyjding@126.com (Q. Zhong)*

[2]*Departments of Chemical and Petroleum Engineering, University of Wyoming, Laramie, Wyoming 82071, USA, mfan@uwyo.edu (M. Fan)*

[3]*Department of Chemical Engineering, Brigham Young University, Provo, UT 84602, USA, mdargyle@byu.edu (M. D. Argyle)*

[4]*Laboratory of Catalysis, Dalian Institute of Chemical Physics, Chinese Academy of Sciences, Dalian, Liaoning 116023, China*

[5]*National Institute of Clean-and-Low-Carbon Energy, P.O. Box 001 Shenhua, NICE, Beijing, China*

[6]*Nanjing Institute of Geography and Limnology, Chinese Academy of Sciences, Nanjing 210008, China*

[7]*School of Civil and Environmental Engineering, Georgia Institute of Technology, Atlanta, GA, 30332, USA*

[8]*School of Chemistry and Chemical Engineering, Henan Polytechnic Universty, Jiaozuo, Henan 45400, China*

S1 Preparation of catalysts

Preparation of Iron-copper catalysts. Iron-copper catalysts were prepared by a hydrothermal method with $Fe(NO_3)_3$•$9H_2O$ (Aladdin, purity ≥ 99.9%) and $Cu(NO_3)_2$•$3H_2O$ (Aladdin, AR) as the Fe and Co sources, respectively, and with urea (Aladdin, purity ≥ 99.5%) as the precipitant agent. Typically, 4.04 g (0.01 mol) $Fe(NO_3)_3$•$9H_2O$, 2.42 g (0.01 mol) $Cu(NO_3)_2$•$3H_2O$ and 3.00 g (0.05 mol) urea were dissolved in 80 mL deionized water. The solutions were transferred into a 100 mL Teflon lined cylinder to react for 12 h at 120 °C. The precipitates were calcined at 500 °C for 4 h to obtain Iron-copper catalysts.

Preparation of Iron-copper-potassium catalysts. Iron-copper-potassium catalysts were prepared by impregnation. Typically, 2 g of iron-copper catalysts were added into 100 mL of deionized water and the desired amount of KNO_3 (Aladdin, purity ≥ 99.0%) was added to the solution. The molar ratio of K/(Fe+Co) used for preparing iron-copper-potassium catalysts was 0, 0.05, 0.10 and 0.15. The mixed solutions were heated at 80 °C until the liquid was evaporated. The obtained material was dried at 120 °C for 12 h. Finally, Iron-copper-potassium catalysts was obtained after calcination at 500 °C for 4 h, which was expressed as $Fe_xCu_yK_z$. The x, y and z represent the molar ratio of iron, copper and potassium, respectively. The $Fe_{0.45}Cu_{0.45}K_{0.10}$ was defined to FCK, and the R-FCK was obtained after being reduced in a flow 37.5 mL/min mixture gas containing 80 vol% H_2 and 20 vol% N_2 at 400 °C for 4 h.

Preparation of SAPO-34. SAPO-34 was synthesized by a hydrothermal method using pseudoboehmite (72 wt% Al_2O_3), orthophosphoric acid (85 wt% H_3PO_4), silica sol (30 wt% SiO_2), and trimethylamine (TEA) as the sources of Al, P, Si, and the template, respectively. The molar ratio of TEA/Al_2O_3/SiO_2/P_2O_5/H_2O in the synthesis gel was 3:1:0.25:1:50. After the hydrothermal synthesis at 200 °C for 72 h, the solid sample was recovered by centrifugation, washing, and drying at 100 °C for 6 h. The sample was calcined in air at 550 °C to remove the organic template.

Preparation of admixed catalysts composed of $Fe_xCu_yK_z$ and SAPO-34. The admixed catalysts were prepared by physical mixing. Typically, 0.1 g $Fe_xCu_yK_z$ and 0.1 g SAPO-34 were mixed, which is defined as $Fe_xCu_yK_z$/SAPO. 1 g $Fe_xCu_yK_z$/SAPO was

obtained after five preparations. The $Fe_{0.45}Cu_{0.45}K_{0.10}$/SAPO-34 is defined as FCK/SAPO. R-FCK/SAPO was obtained by reducing FCK/SAPO at 400 °C under 80 vol% H_2/20 vol% N_2 for 4 h.

Preparation of Cu-Fe alloy and Fe-Cu alloy. For the preparation of Cu-Fe alloy, 5.61 g of $Fe(NO_3)_3 \cdot 9H_2O$ and 0.84 g of $Cu(NO_3)_2 \cdot 3H_2O$ were dissolved in 100 mL distilled H_2O under stirring. The above solution was heated to 80 °C under stirring until it was dried. The obtained precipitation was calcined at 500 °C, and then it was reduced at 400 °C under the H_2 atmosphere to obtain Cu-Fe alloy. For the preparation of Fe-Cu alloy, 0.64 g of $Fe(NO_3)_3 \cdot 9H_2O$ and 3.44 g of $Cu(NO_3)_2 \cdot 3H_2O$ were dissolved in 100 mL distilled H_2O under stirring. The above solution was heated to 80 °C under stirring until it was dried. The obtained precipitation was calcined at 500 °C, and then it was reduced at 400 °C under the H_2 atmosphere to obtain Fe-Cu alloy.

S2 Characterization of Catalysts

The scanning electron microscopy (SEM) and energy dispersive spectroscopy (EDS) characterizations were performed with Hitachi S-4800II instrument. High-resolution Transmission Electron Microscopy (HRTEM) characterization was conducted on a Tecnai G2 S-Twin F30 TEM operated at 200 kV. X-ray diffraction (XRD) patterns and in-situ XRD patterns were recorded on a Bruker D2 Phaser with Cu Kα radiation (36 kV voltage and 30 mA) as the X-ray source. X-ray photoelectron spectroscopy (XPS) was tested on a Kratos Axis Ultra DLD equipment with a monochromated Al K-alpha source with an error of 0.1 eV. ^{57}Fe Mössbauer spectra were acquired in an MR-351 constant-acceleration Mössbauer spectrometer (FSAT, Germany) drive with a triangular reference signal at room temperature. In-situ infrared (IR) spectra were conducted using Nicolet 6700 spectrometer with a resolution of 4 cm^{-1}, and all the prepared catalysts were reduced at 400 °C in a flowing 37.5 mL/min H_2-N_2 mixture (80 vol.% H_2) for 4 h, followed by evacuating the prepared catalysts for 30 min to remove the physiosorbed H_2 and N_2 prior to characterization. Pyridine-IR spectra were also obtained on a Nicolet 6700 spectrometer with a resolution of 4 cm^{-1}. The concentration of different phases were calculated from GSAS program.

H_2 temperature-programmed desorption/reduction (H_2-TPD/H_2-TPR). H_2 temperature-programmed desorption/reduction (H_2-TPD/H_2-TPR) were performed with a Micromeritics Autochem II 2920 instrument. For H_2-TPD, 0.12 g prepared catalysts were first reduced at 400 °C in a flowing 37.5 mL/min H_2-N_2 mixture (80 vol% H_2) for 4 h, and then the adsorption tests were conducted at 40 °C in a flowing 37.5 mL/min 100 vol% H_2 for 4 h. The desorption tests were conducted in a flowing 37.5 mL/min Ar with the temperature increase from room temperature to 900 °C at 10 °C/min. For H_2-TPR, 0.12 g prepared catalysts were used in a flowing 37.5 mL/min H_2-Ar mixture (10 vol.% H_2) with the temperature increase from room temperature to 900 °C at 10 °C/min.

CO_2 or H_2 pulse experiments. CO_2 or H_2 pulse experiments were used to measure CO_2 and H_2 adsorption rates, which was conducted in a temporal analysis of products (TAP) reactor with setting the valve to generate ~6.0×10^{11} molecules per pulse. The prepared catalysts were first pretreated at 400 °C in a flowing 37.5 mL/min H_2-N_2 mixture (80 vol.% H_2) for 1 h, and then the prepared catalysts were tested at 340 °C or 370 °C in a flowing 1 mL/min CO_2-Ar or H_2-Ar mixtures containing 0.001% CO_2 or H_2. The differentially pumped gate valve was used to propagate CO_2/Ar or H_2/Ar mixtures into the analysis chamber, and the quadrupole mass spectrometer was used to quantify CO_2 or H_2 concentration

CO_2 temperature-programmed desorption (CO_2-TPD). CO_2 temperature-programmed desorption (CO_2-TPD) was performed with a Micrometrics Autochem II 2920. 0.12 g prepared catalysts were first reduced at 400 °C in a flowing 37.5 mL/min H_2-N_2 mixture (80 vol% H_2) for 4 h, and then the adsorption tests were conducted at 40 °C in a flowing 37.5 mL/min 100 vol% CO_2 for 4 h. The desorption tests were conducted in a flowing 37.5 mL/min He with the temperature increase from room temperature to 900 °C at 10 °C/min.

S3 DFT calculation

Density functional theory calculations were carried out using VASP with the gradient-corrected PBE exchange-correction function[1-3]. In the calculation, a slab

model containing 4 formula units of metal oxides was employed, and a vacuum of 10 Å was set to simulate the surface in periodic boundary conditions; a 4×4×1 Monkhorst-Pack grid was used in the *k*-point sampling for the surface calculation. The energy cut off for the plane-waves was set to 450 eV[1,2]. Cu-Fe alloy models substituted top-layer Fe atoms with different numbers of Cu atoms[2,4-6]. The adsorption energy was calculated by:

$$E_{ad} = E_{sm} - E_{surf} - E_{mol}$$

where E_{sm} is the calculated total energy of reactants adsorbed on the surface, E_{surf} is the calculated energy of catalyst surface and E_{mol} is the calculated energy of reactants.

S4 Catalytic tests

The fixed-bed reactor was used to test the activities of prepared catalysts as previously reported[7]. Briefly, 1 g prepared catalysts were loaded into the reactor, and they were reduced at 400 °C in a flowing 37.5 mL/min H_2-N_2 mixture (80 vol.% H_2) for 4 h. After reduction, the prepared catalysts were tested at the reaction pressure of 1.5 MPa and the reaction temperature range from 300 to 400 °C in a flowing 25 mL/min CO_2-H_2 mixtures (the volume ratio of CO_2 to H_2 is 1/4).

The products were analyzed by an online gas chromatograph with three channels, which installed two packed columns and two capillary columns. The first channel, used H_2 as the carrier gas, was equipped with a cascaded of a Porpak Q column (1 m), a 5 A molecular sieve column (5 m) and a thermal conductivity detector (TCD), which was used to analyze the CO and CO_2. The second channel, used highly pure N_2 as the carrier gas, was equipped with a cascaded of a Al_2O_3 capillary column (30 m × 0.53 mm × 20 μm) and a FID detector to analyze CH_4, C_2H_4, C_2H_6, C_3H_6, C_3H_8, C_4H_8, C_4H_{10}, C_5H_{10} and other hydrocarbons. The third channel, used highly pure N_2 as the carrier gas, was equipped with a cascaded of a PEG20000 capillary column (30 m × 0.53 mm × 20 μm) and a FID detector to analyze methanol. The conversion (X, %), space time yields (STY, $mmol \cdot g^{-1}_{cat} \cdot h^{-1}$), selectivities (S, %), and yields (%) were defined as follows:

$$X_{CO_2} = (1 - \frac{C_{CO_2,in} \cdot f_{in} - C_{CO_2,out} \cdot f_{out}}{C_{CO_2,in} \cdot f_{in}})$$

$$S_{C_n} = \frac{C_{C_n,out}}{C_{CO} + C_{C_1,out} + C_{C_2,out} + \ldots + C_{C_n,out} + \ldots}$$

$$STY_{C_2^= - C_4^=} = \frac{X_{CO_2}/100 \cdot S_{C_2^= - C_4^=}/100 \cdot GHSV_{CO_2}}{22.4}$$

where $C_{CO_2,in}$ and $C_{CO_2,out}$ are the inlet and outlet concentrations of CO_2, respectively, which are determined by GC analysis. f_{in} and f_{out} are the inlet and outlet flow of the fixed-bed reactor, respectively. C_{CO}, $C_{C_1,out}$, $C_{C_2,out}$, …, $C_{C_n,out}$ are the outlet concentrations of CO, C_1, C_2, …, C_n compounds determined by GC analysis, respectively. The carbon balance, CBE, evaluated by the following equation, which was ≥ 95% in every test:

$$CBE = \frac{C_{CO} + C_{C_1,out} + 2 \times C_{C_2,out} + \ldots + n \times C_{C_n,out} + \ldots}{C_{CO_2,in} \cdot f_{in} - C_{CO_2,out} \cdot f_{out}}$$

S5. Optimizations of catalytic performances

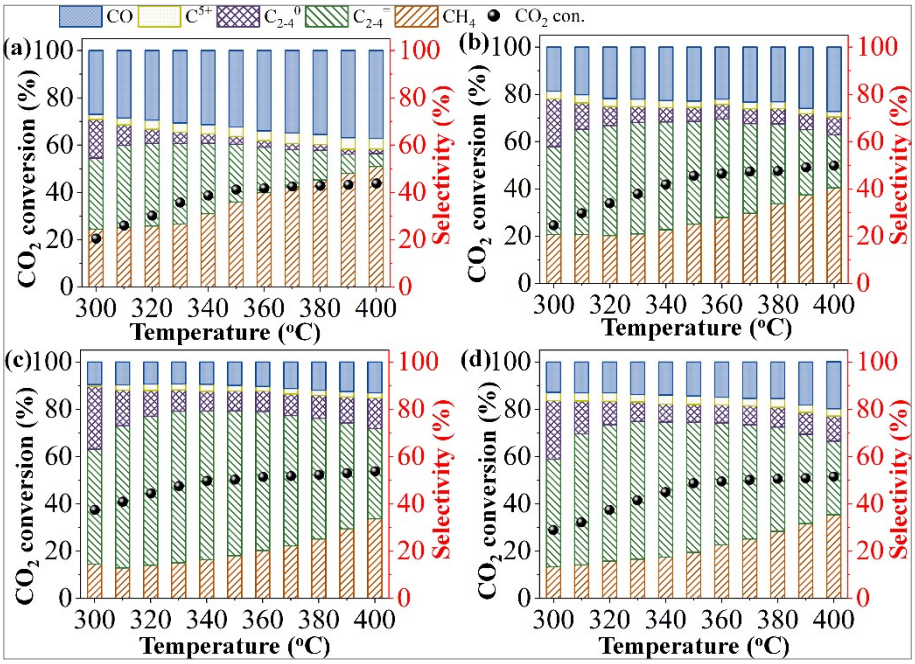

Fig. S1. Effect of K loading on catalytic activity [(a) $Fe_{0.5}Cu_{0.5}$/SAPO-34; (b) $Fe_{0.475}Cu_{0.475}K_{0.050}$/SAPO-34; (c) $Fe_{0.45}Cu_{0.45}K_{0.10}$/SAPO-34; (d) $Fe_{0.425}Cu_{0.425}K_{0.150}$ /SAPO-34. Mass ratio of $Fe_xCu_yK_z$/SAPO-34: 1/1; Molar ratios of Fe/Cu: 1/1; GHSV: 1500 mL·h^{-1}·g^{-1}; P: 1.5 MPa]

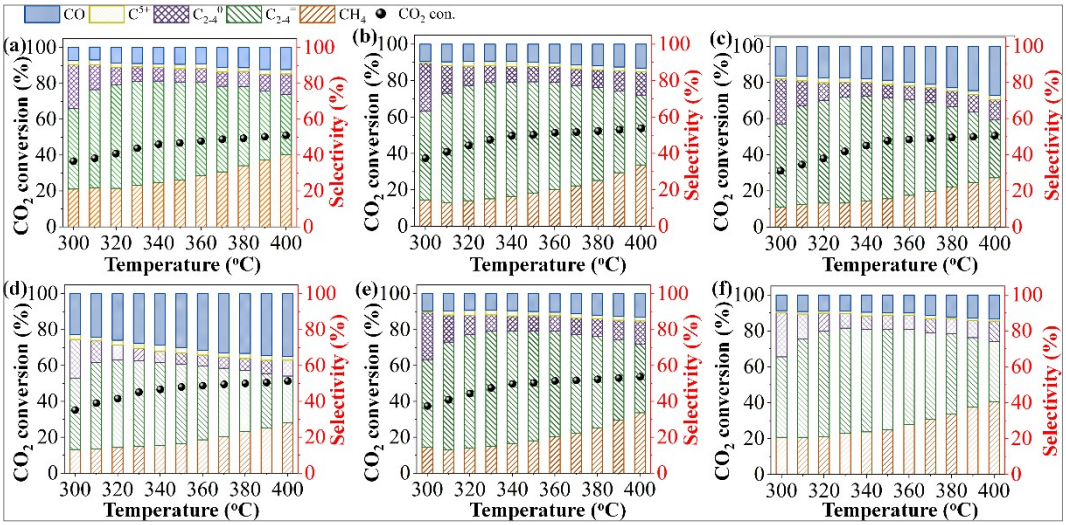

Fig. S2. Effect of Fe/Cu molar ratios and $Fe_xCu_yK_z$ to SAPO-34 mass ratios on catalytic activity [(a) $Fe_{0.675}Cu_{0.225}K_{0.100}$/SAPO-34; (b) $Fe_{0.45}Cu_{0.45}K_{0.10}$/SAPO-34; (c) $Fe_{0.225}Cu_{0.675}K_{0.100}$ /SAPO-34. Mass ratio of $Fe_xCu_yK_z$/SAPO-34: 2/1; K loading: 10 wt%; GHSV: 1500 mL·h^{-1}·g^{-1}; P: 1.5 MPa. (d) $Fe_{0.45}Cu_{0.45}K_{0.10}$/SAPO-34 with mass ratio of 2/1; (e) $Fe_{0.45}Cu_{0.45}K_{0.10}$/SAPO-34 with mass ratio of 1/1; (f)

$Fe_{0.45}Cu_{0.45}K_{0.10}$/SAPO-34 with mass ratio of 1/2. Molar ratio of Fe/Cu: 1/1; K loading: 10 wt%; GHSV: 1500 $mL \cdot h^{-1} \cdot g^{-1}$; P: 1.5 MPa]

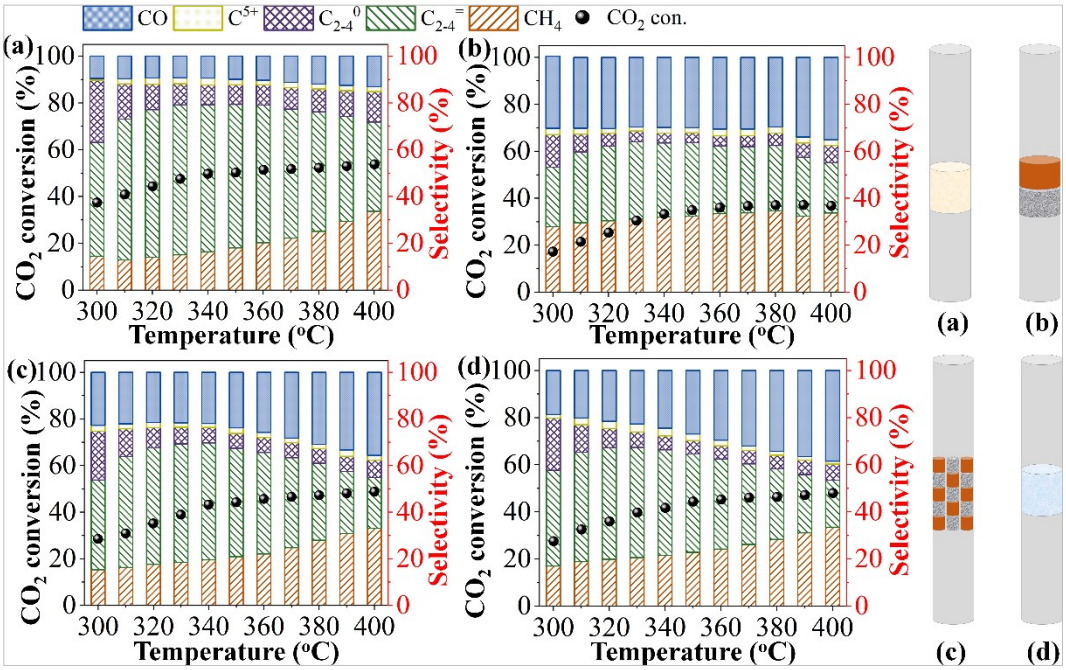

Fig. S3. Effect of loading method on catalytic activity [Right: catalytic activities; Left: loading method; (a) $Fe_xCu_yK_z$ mixed with SAPO-34; (b) SAPO-34 followed with $Fe_xCu_yK_z$; (c) Large $Fe_xCu_yK_z$ particle mixed with large SAPO-34 particle; (d) $Fe_xCu_yK_z$ mixed with SiO_2 and SAPO-34. Mass ratio of $Fe_xCu_yK_z$/SAPO-34: 1/1; Molar ratio of Fe/Cu: 1/1; K loading: 10 wt%; GHSV: 1500 $mL \cdot h^{-1} \cdot g^{-1}$; P: 1.5 MPa]

S6. Effects of GHSV and particle sizes on catalytic activity, and mass spectra

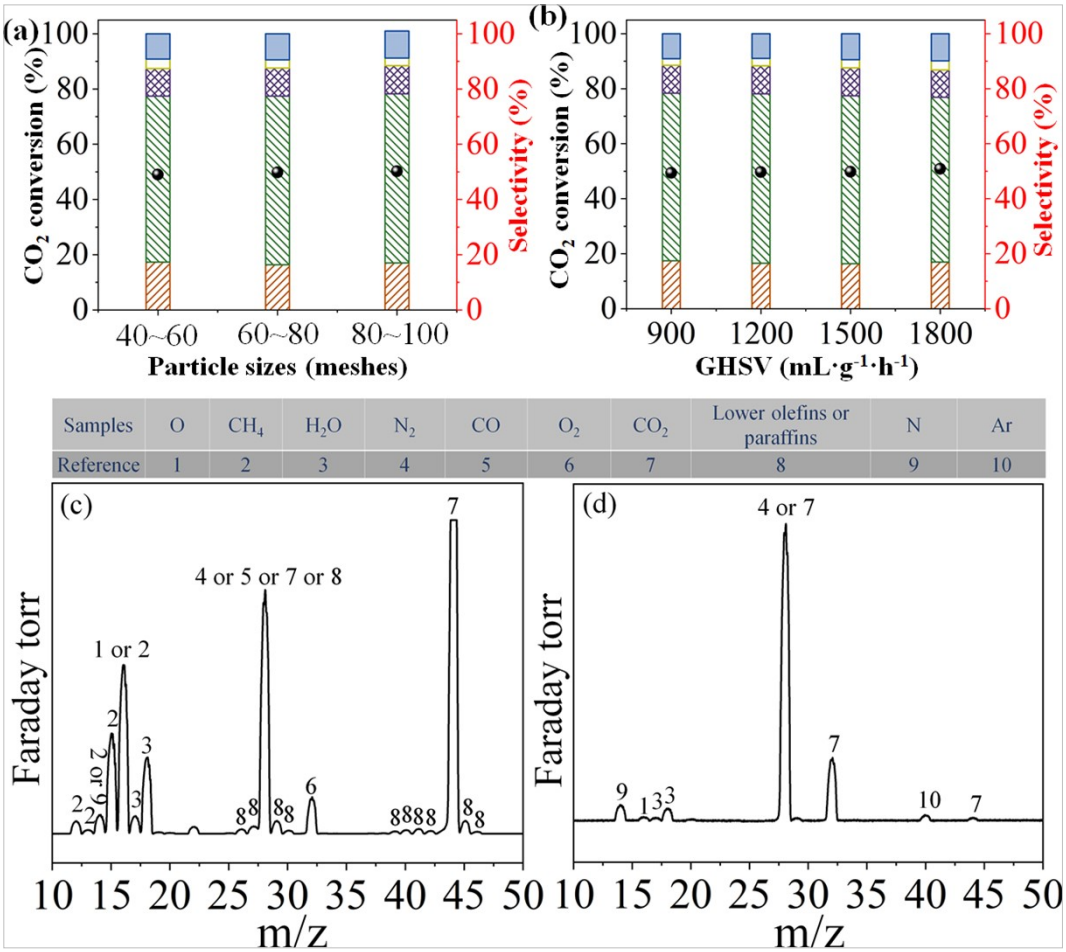

Samples	O	CH_4	H_2O	N_2	CO	O_2	CO_2	Lower olefins or paraffins	N	Ar
Reference	1	2	3	4	5	6	7	8	9	10

Fig. S4. Effect of particle sizes and GHSV on catalytic activity, and mass spectra of products from catalytic CO_2 hydrogenation and air [Mass ratio of $Fe_xCu_yK_z$/SAPO-34: 1/1; Molar ratio of Fe/Cu: 1/1; K loading: 10 wt%; GHSV: 1500 mL·h^{-1}·g^{-1}; P: 1.5 MPa. Mass spectra of (c) products from CO_2 hydrogenation and (d) Air]

S7. Lower olefins yield and effect of NO on catalytic performances

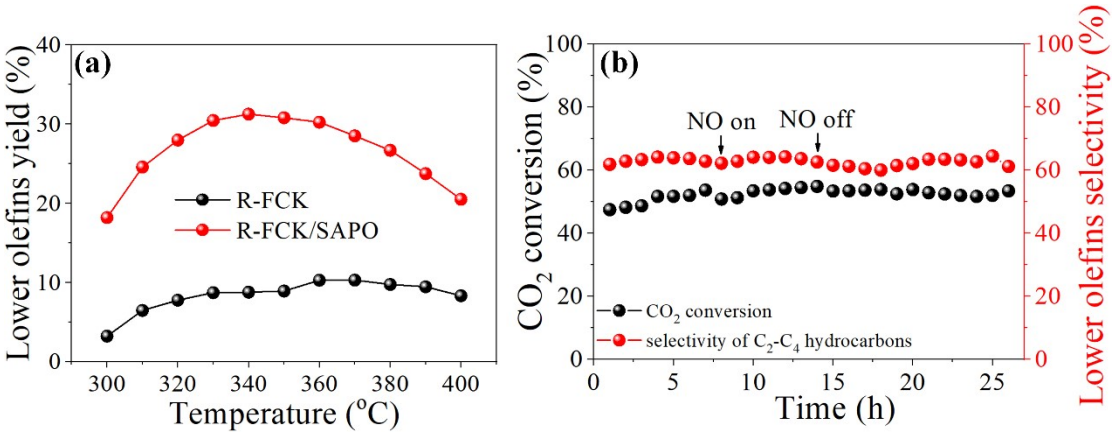

Fig. S5. Performances and characterizations of prepared catalysts. [(a) Lower olefins yield; (b) effect of NO on CO_2 conversion and selectivity]

S8. Summary of performance for CO_2 hydrogenation to lower olefins

Table S1. Summary of performance for CO_2 hydrogenation to lower olefins

Catalyst	T (°C)	P (MPa)	X_{CO2} (%)	$S_{C2-4}^{=}$ (%)	S_{CO} (%)	STY (mmol•g$^{-1}_{cat}$•h^{-1})
R-FCK/SAPO	330	1.50	47.52	62.90	9.66	4.19
$ZnZrO_X$/SAPO[8]	380	2.00	12.60	65.04	~43	3.29
$InZrO_X$/SAPO[9]	400	3.00	35.50	48.85	≥80	4.12
$ZnGa_2O_4$/SAPO[10]	400	3.00	13.00	56.21	~67	3.29
CeO_2-Pt@SiO_2-Co[11]	250	6.21	3.00	40.00	~20	1.03
$CuFeO_2$[12]	300	1.00	18.10	39.70	~30	1.32
Co-Fe catalysts[13]	220	0.92	27.20	13.20	~50	2.94×10^{-6}
FeSiKCu[14]	500	1.30	15.00	65.00	NG	2.18
Cu-Zn-Al/HB[15]	300	0.98	27.64	43.20	53.40	4.00
Fe_3O_4/γ-Fe_2O_3[16]	300	1.00	38.00	35.00	~12	4.01
Fe-Zn-K[17]	320	0.50	37.76	48.89	11.13	4.12
Fe_2O_3/MOF[18]	300	3.00	25.00	45.00	~20	4.14
Fe-Co/K[19]	300	1.10	31.00	30.00	~20	0.66
Fe-Zn-Cu[20]	275	1.00	39.80	39.80	~10	0.81

Note: “NG” means “not given”

S9. EDS of R-FCK and R-FCK/SAPO

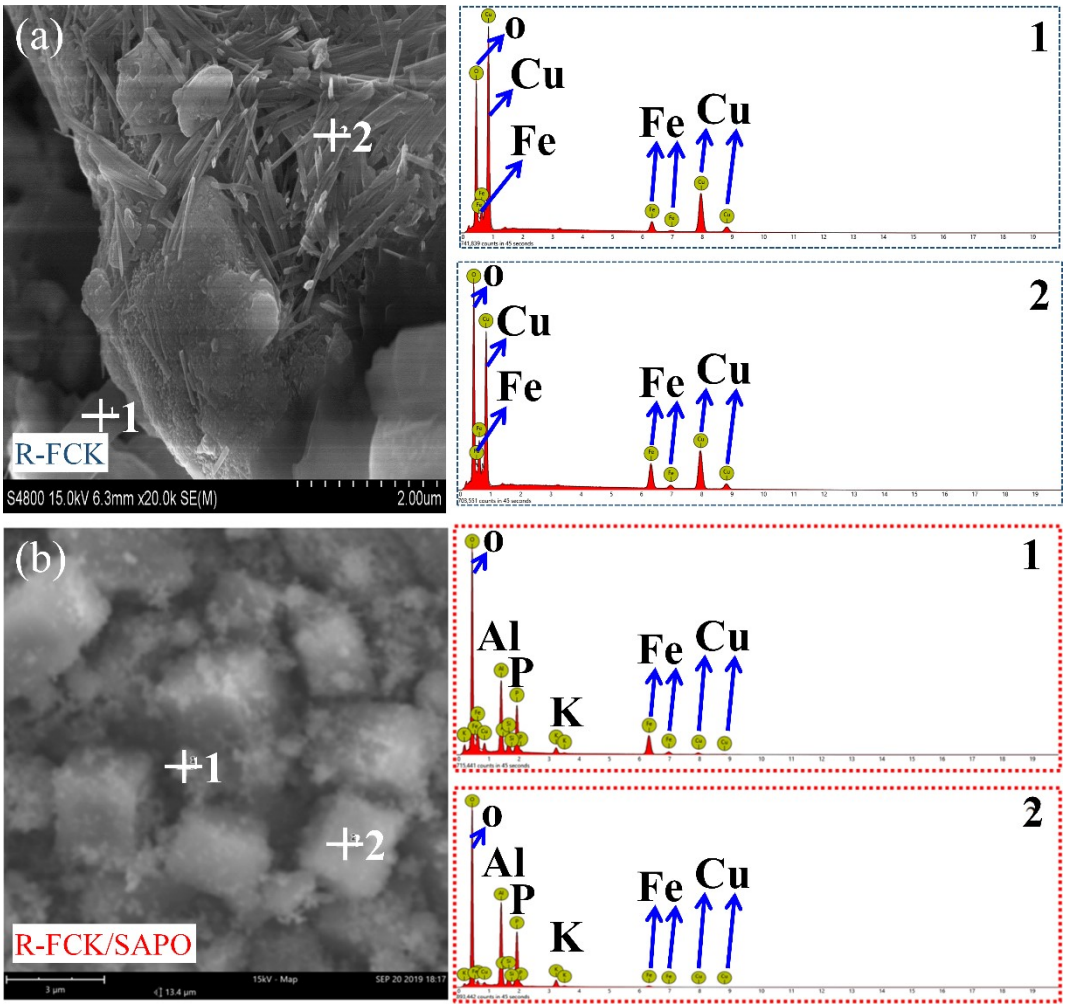

Fig. S6. EDS of R-FCK (1: Cu 90.68 mol.%; 2: Cu 21.05 mol.%) and R-FCK/SAPO (1: Cu 14.80 mol.%)

The elemental analysis of the second dot in Fig. S6b is not accurate because it contains amounts of Si, Al and P elements.

S10. XRD patterns of R-FCK, R-FCK/SAPO, pure Cu and pure Fe

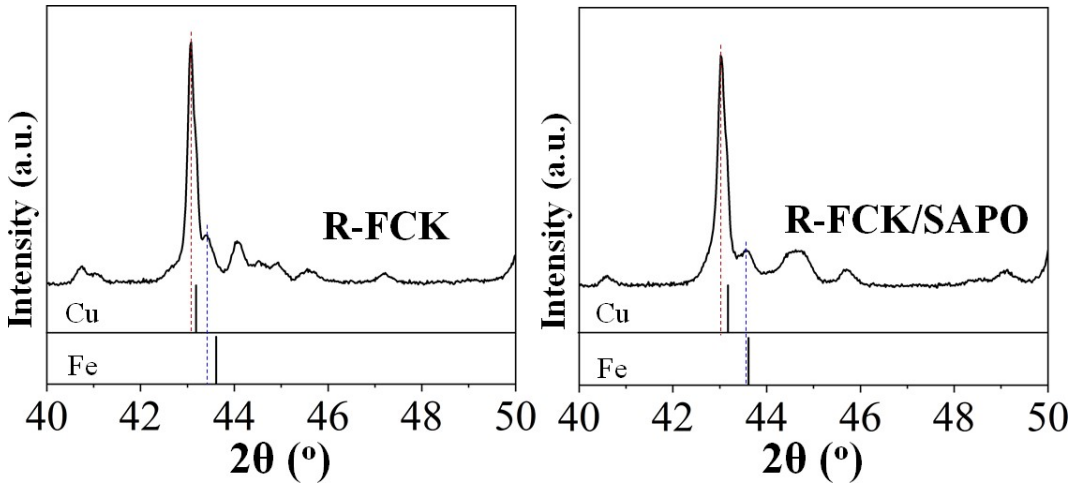

Fig. S7. XRD patterns of R-FCK, R-FCK/SAPO, pure Cu and pure Fe

S11. Catalytic performances of Cu-Fe alloy and Fe-Cu alloy

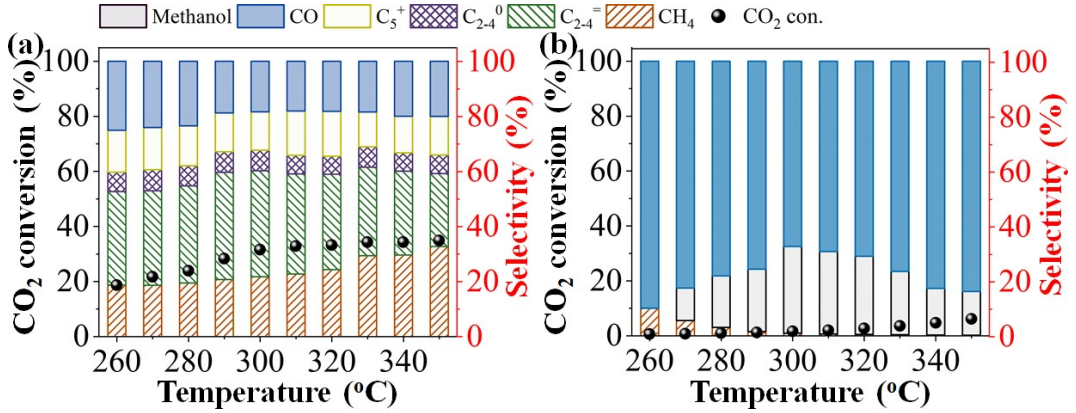

Fig. S8. Catalytic performances of (a) Cu-Fe alloy with 9.32 mol.% Cu and (b) Fe-Cu alloy with 21.05 mol.% Fe.

S12. HRTEM image of fractured nanorods

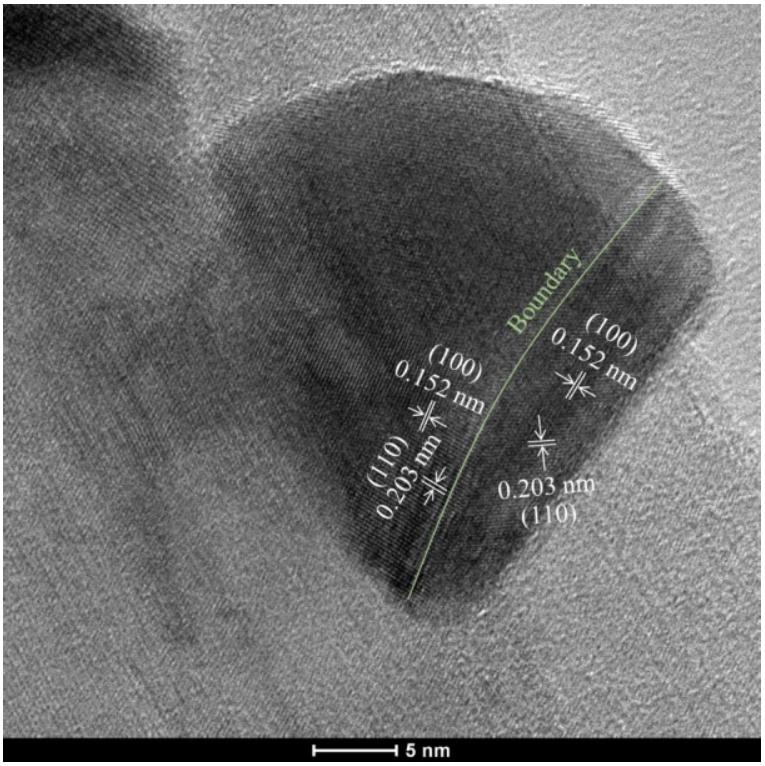

Fig. S9. HRTEM image of fractured nanorods

S13. EDS images of R-FCK/SAPO and Cu2p XPS

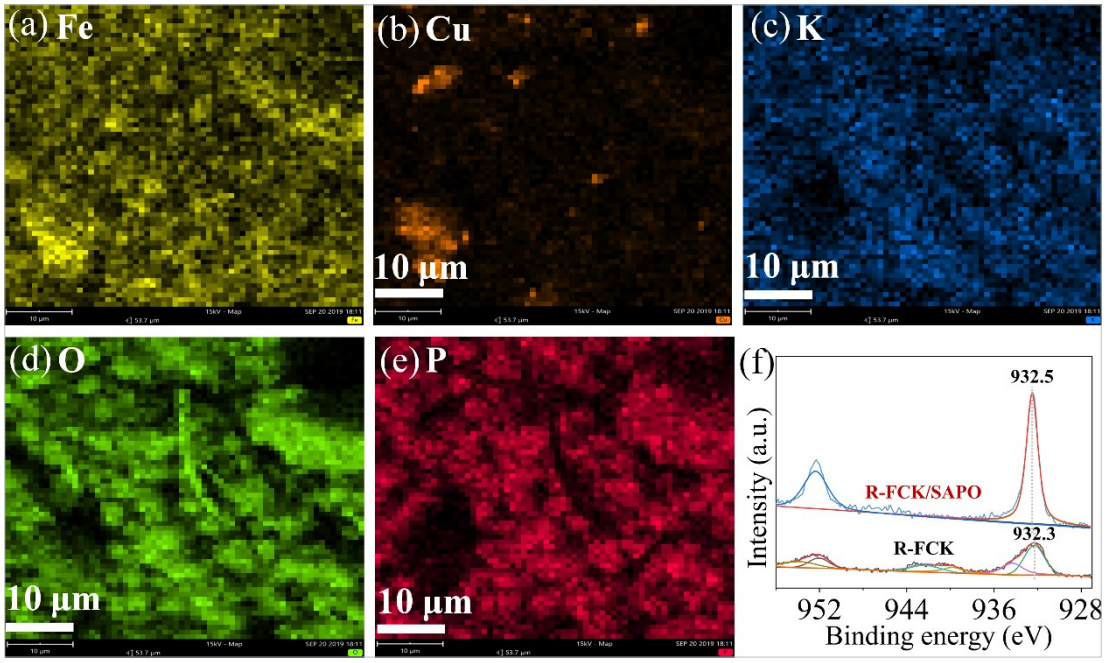

Fig. S10. EDS image of R-FCK/SAPO and Cu2p XPS

S14 Elemental analysis of R-FCK and R-FCK/SAPO from XPS and AES

Table S2 Surface compositions of R-FCK and R-FCK/SAPO

Samples	Fe/%	Fe^0/%	Fe^{2+}/%	Fe^{3+}/%	Cu/%	Cu^0/%	Cu^+/%	Cu^{2+}/%
R-FCK	5.60	1.62	2.00	1.98	3.08	0.29	1.13	1.66
R-FCK/SAPO	3.36	1.20	1.25	0.91	2.04	0.76	1.28	0
Samples	K/%				O/%			
R-FCK	27.03				64.29			
R-FCK/SAPO	1.74				39.02			

S15. Calculation process of different Fe crystal planes on R-FCK and R-FCK/SAPO

According to the literature, the weight percentage of one phase can be calculated according to the following equation:

$$w_i = \frac{S_i M_i V_i}{\sum_j S_j M_j V_j} \quad \text{(S-1)}$$

S_i is referred to scale factor; M_i is referred to the cell mass; V_i is referred to the cell volume.

S_i is positive to the peak intensity, which can be calculated as follows:

$$I_{hkl} = S \cdot M_{hkl} \cdot L_{hkl} \cdot |F_{hkl}| \quad \text{(S-2)}$$

I_{hkl} is referred to the absolute intensity of peak, which means the difference between the intensity and the background; M_{hkl} is referred to the multiplicity factor; L_{hkl} is referred to Lorentz factor; $|F_{hkl}|$ is referred to structural amplitude.

For the Fe in R-FCK/SAPO, the Fe (110) and Fe (100) are two planes of cubic Fe phase. Both are in the same cell with different planes. Therefore, the W_i is directly relative to I_{hkl}, and the W_i is also equal to molar ratio (n_i).

$$\frac{n_{(110)}}{n_{(100)}} = \frac{I_{(110)}}{I_{(100)}} = \frac{1782 - 580}{729 - 580} = 5.25$$

From the XRD patterns, the Fe in R-FCK/SAPO is mainly consisted of Fe (110) and Fe (100). Therefore, the molar percentage of Fe (110) phase is 84.0% and the one of Fe (100) is 16.0%.

For the Fe in R-FCK, the molar ratio of different Fe crystal planes is calculated as follows:

$$\frac{n_{(110)}}{n_{(100)}} = \frac{I_{(110)}}{I_{(100)}} = \frac{1689 - 692}{944 - 839} = 1.34$$

Therefore, the molar percentage of Fe (110) phase is 57.3% and the one of Fe (100) is 42.7%.

S16. Detailed description of H_2-TPR profiles

H_2-TPR profiles of SAPO, R-FCK and R-FCK/SAPO are shown in Fig. S11. SAPO displays almost no hydrogen consumption, indicating that the SAPO is stable under the H_2 atmosphere at the reduction and reaction temperature. FCK presents a large peak ranging from 350 to 620 °C, with a small but wide shoulder at 620-750 °C. The former one is assigned to the reduction of Fe_2O_3/CuO to Fe_3O_4/Cu_2O and the complete reduction of well-dispersed Fe_2O_3/CuO particles to Fe/Cu. The latter one is attributed to the reduction of Fe_3O_4/Cu_2O to FeO or Fe/Cu. FCK can only be partially reduced at the reduction temperature (400 °C) and reaction temperature (300-400 °C), resulting in Fe_3O_4/Cu_2O and well-dispersed Fe/Cu particles on the catalyst surface. FCK-SAPO displays a main peak at 270-450 °C, with a wide shoulder at 450-800 °C. These two peaks for R-FCK/SAPO have similar attributions to the peaks for FCK. However, the FCK-SAPO peaks shift to the lower temperature in comparison to those for FCK, which is due to the good dispersion of Fe and Cu species on the SAPO surface.

S17. Surface compositions of R-FCK and R-FCK/SAPO from XPS and AES

Table S3 Surface compositions of R-FCK and R-FCK/SAPO from XPS and AES

Samples	Fe^0/%	Fe^{2+}/%	Fe^{3+}/%	Cu^0/%	Cu^+/%	Cu^{2+}/%
R-FCK	29.07	35.63	35.29	9.44	36.60	53.96
R-FCK/SAPO	35.62	37.23	27.15	37.35	65.65	0

S18. Physical properties of fresh and reduced catalysts

Table S4 BET surface areas, pore volumes and pore sizes of catalysts

Samples	BET surface areas (m^2/g)	Pore volumes (cm^3/g)	Pore sizes (nm)
SAPO	439.2	0.00599	14.9
FCK	38.36	0.0321	29.8
FCK/SAPO	137.64	0.0272	10.9
R-FCK	29.33	0.0296	38.1
R-FCK/SAPO	117.0	0.0203	14.5

S19. Detailed description of CO_2-TPD profiles

The CO_2-TPD profiles of R-FCK, R-FCK/SAPO, and SAPO are shown in Fig. 3j. Both R-FCK-SAPO and R-FCK have three peaks at 101-128 °C, 251-272 °C and 697-768 °C, while SAPO exhibits only one peak at 167 °C. The peaks at the low temperature (101-167 °C) are attributed to physical adsorption of CO_2. The peaks at medium temperature (251-272 °C) are attributed to chemical adsorption of CO_2, which results from the adsorption of CO_2 on surface -OH and surface defects. The peaks at high temperature (697-768 °C) result from the loss of lattice oxygen.

S20. H_2 adsorption capacity v.s. reaction temperature and H_2 adsorption rates

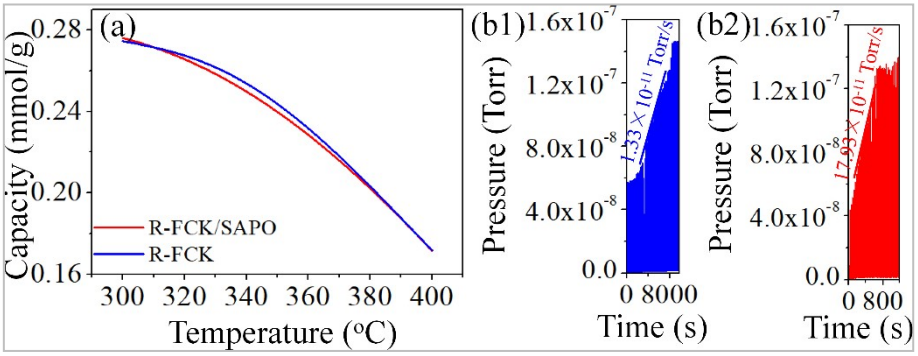

Fig. S11. (a) H_2 adsorption capacity v.s. reaction temperature; H_2 adsorption rates of (b1) R-FCK and (b2) R-FCK/SAPO.

S21. Carbon number distributions at optimal reaction temperature

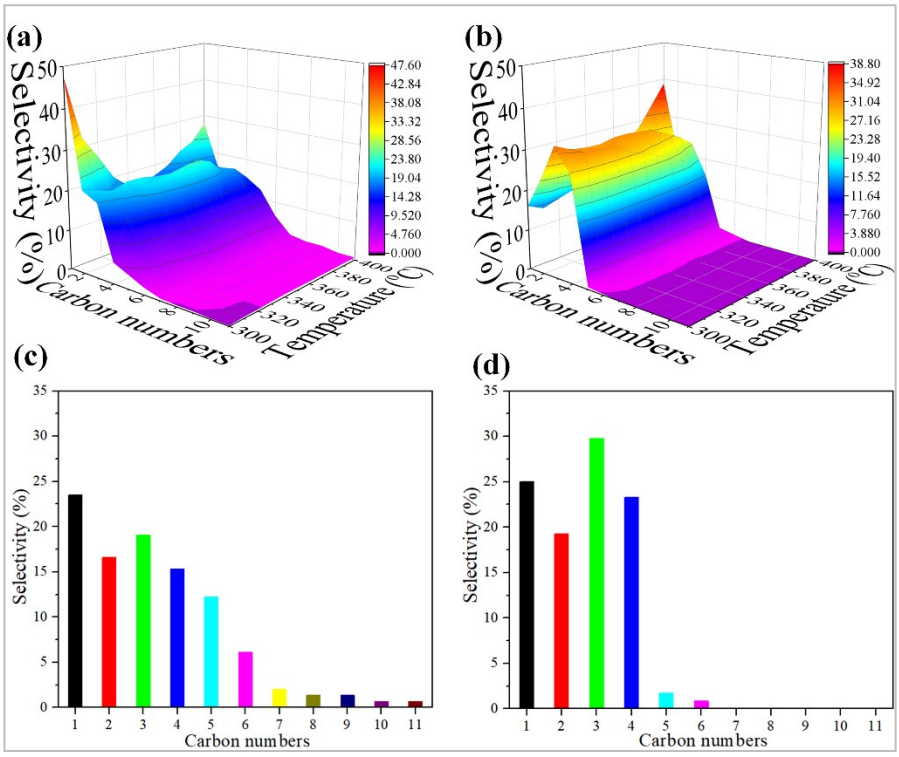

Fig. S12. Carbon number distributions at optimal reaction temperature [(a) R-FCK at 370 °C; (b) R-FCK/SAPO at 340 °C]

S22. Catalytic dehydration of methanol over SAPO

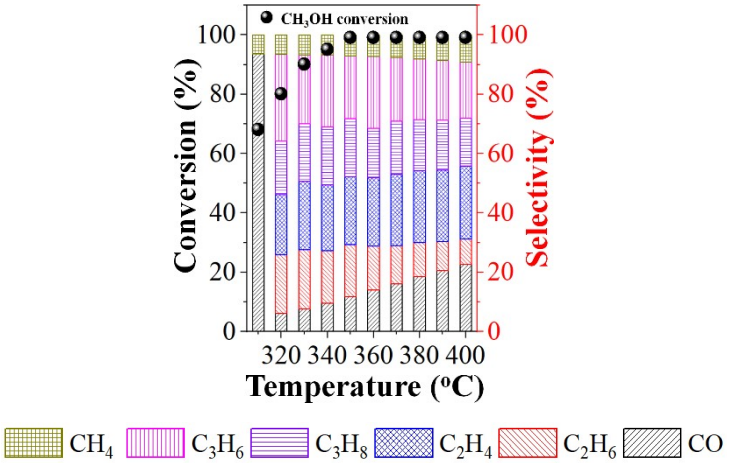

Fig. S13 Catalytic dehydration of methanol over SAPO

References

1. Nie, X.; Wang, H.; Janik, M. J.; Chen, Y.; Guo, X.; Song, C. Mechanistic insight into C-C coupling over Fe-Cu bimetallic catalysts in CO_2 hydrogenation. *Journal of Physical Chemistry C* **2017**, *121*, 13164-13174.

2. Nie, X.; Wang, H.; Janik, M. J.; Guo, X.; Song, C. Computational investigation of Fe-Cu bimetallic catalysts for CO_2 hydrogenation. *Journal of Physical Chemistry C* **2016**, *120*, 9364-9373.

3. Hwang, S. -M.; Han, S. J.; Min, J. E.; Park, H. G.; Jun, K. -W.; Kim, S. K. Mechanistic insights into Cu and K promoted Fe-catalyzed production of liquid hydrocarbons via CO_2 hydrogenation. *Journal of CO_2 Utilization* **2019**, 34, 522-532.

4. K. Ray, G. Deo, A potential descriptor for the CO_2 hydrogenation to CH_4 over Al_2O_3 supported Ni and Ni-based alloy catalysts. Applied Catalysis B: Environmental, 2017, 218, 525-537.

5. Y. Wang, H. Gao, J. Wang, Y. Han, Y. Dai, B. Sun, First-principles calculations of Ag addition on the diffusion mechanisms of Cu-Fe alloys. Solid State Communications, 2014, 183, 60-63.

6. M. Elahifard, A. Fazeli, A. Joshani, M. Gholami, Ab-Initio calculations of the CO adsorption and dissociation on substitutional Fe–Cu surface alloys relevant to Fischer–Tropsch Synthesis: bcc-(Cu)Fe(100) and fcc-(Fe)Cu(100). Surface and Interface Analysis, 2013, 45, 1081-1087.

7. Ding, J.; Huang, L.; Gong, W.; Fan, M.; Zhong, Q.; Russell, A. G.; Gu, H.; Zhang, H.; Zhang, Y.; Ye, R.-p., CO_2 hydrogenation to light olefins with high-performance $Fe_{0.30}Co_{0.15}Zr_{0.45}K_{0.10}O_{1.63}$. *Journal of Catalysis* **2019,** *377*, 224-232.

8. Li, Z.; Wang, J.; Qu, Y.; Liu, H.; Tang, C.; Miao, S.; Feng, Z.; An, H.; Li, C., Highly Selective conversion of carbon dioxide to lower olefins. *ACS Catalysis* **2017,** *7* (12), 8544-8548.

9. Gao, P.; Dang, S.; Li, S.; Bu, X.; Liu, Z.; Qiu, M.; Yang, C.; Wang, H.; Zhong, L.; Han, Y.; Liu, Q.; Wei, W.; Sun, Y., Direct production of lower olefins from CO_2 conversion via bifunctional catalysis. *ACS Catalysis* **2018,** *8* (1), 571-578.

10. Liu, X.; Wang, M.; Zhou, C.; Zhou, W.; Cheng, K.; Kang, J.; Zhang, Q.; Deng, W.; Wang, Y., Selective transformation of carbon dioxide into lower olefins with a bifunctional catalyst composed of $ZnGa_2O_4$ and SAPO-34. *Chemical Communications* **2018,** *54* (2), 140-143.

11. Xie, C.; Chen, C.; Yu, Y.; Su, J.; Li, Y.; Somorjai, G. A.; Yang, P., Tandem Catalysis for CO_2 Hydrogenation to C_2-C_4 Hydrocarbons. *Nano Letters* **2017,** *17* (6), 3798-3802.

12. Choi, Y. H.; Jang, Y. J.; Park, H.; Kim, W. Y.; Lee, Y. H.; Choi, S. H.; Lee, J. S., Carbon dioxide Fischer-Tropsch synthesis: A new path to carbon-neutral fuels. *Applied Catalysis B: Environmental* **2017,** *202*, 605-610.

13. Gnanamani, M. K.; Jacobs, G.; Hamdeh, H. H.; Shafer, W. D.; Liu, F.; Hopps, S. D.; Thomas, G. A.; Davis, B. H., Hydrogenation of carbon dioxide over Co-Fe bimetallic catalysts. *ACS Catalysis* **2016,** *6* (2), 913-927.

14. Shafer, W. D.; Jacobs, G.; Graham, U. M.; Hamdeh, H. H.; Davis, B. H., Increased CO_2 hydrogenation to liquid products using promoted iron catalysts. *Journal of Catalysis* **2019,** *369*, 239-248.

15. Fujiwara, M.; Satake, T.; Shiokawa, K.; Sakurai, H., CO_2 hydrogenation for C_2^+ hydrocarbon synthesis over composite catalyst using surface modified HB zeolite. *Applied Catalysis B: Environmental* **2015,** *179*, 37-43.

16. Visconti, C. G.; Martinelli, M.; Falbo, L.; Infantes-Molina, A.; Lietti, L.; Forzatti, P.; Iaquaniello, G.; Palo, E.; Picutti, B.; Brignoli, F., CO_2 hydrogenation to lower

olefins on a high surface area K-promoted bulk Fe-catalyst. *Applied Catalysis B: Environmental* **2017,** *200*, 530-542.

17. Zhang, J.; Lu, S.; Su, X.; Fan, S.; Ma, Q.; Zhao, T., Selective formation of light olefins from CO2 hydrogenation over Fe-Zn-K catalysts. *Journal of CO_2 Utilization* **2015,** *12*, 95-100.

18. Hu, S.; Liu, M.; Ding, F.; Song, C.; Zhang, G.; Guo, X., Hydrothermally stable MOFs for CO_2 hydrogenation over iron-based catalyst to light olefins. *Journal of CO_2 Utilization* **2016,** *15*, 89-95.

19. Satthawong, R.; Koizumi, N.; Song, C.; Prasassarakich, P., Light olefin synthesis from CO_2 hydrogenation over K-promoted Fe-Co bimetallic catalysts. *Catalysis Today* **2015,** *251*, 34-40.

20. Kim, J.-S.; Lee, S.; Lee, S.-B.; Choi, M.-J.; Lee, K.-W., Performance of catalytic reactors for the hydrogenation of CO_2 to hydrocarbons. *Catalysis Today* **2006,** *115* (1), 228-234.